Calculating Hamiltonian parameters for Yb^{3+} in a low-symmetry lattice site, and fitting the structure and levels of Yb^{3+}:$RETaO_4$ (RE = Gd, Y, and Sc)*

Zhang Qing-Li(张庆礼)†, Ning Kai-Jie(宁凯杰), Ding Li-Hua(丁丽华), Liu Wen-Peng(刘文鹏), Sun Dun-Lu(孙敦陆), Jiang Hai-He(江海河), and Yin Shao-Tang(殷绍唐)

The Key Laboratory of Photonic Devices and Materials of Anhui Province, Anhui Institute of Optics and Fine Mechanics, Chinese Academy of Sciences, Hefei 230031, *China*

(Received 3 October 2012; revised manuscript received 27 December 2012)

An iterative method is used to find the values of the Hamiltonian parameters for Yb^{3+} in a given low-symmetry crystalline site. Samples of Yb^{3+}:$RETaO_4$ (RE = Gd, Y, and Sc) were prepared and their structures were determined. Based on the obtained structural data, their orbital-spin parameters and crystal field parameters were fitted by the superposition model (SM). Using the crystal field parameters obtained by the SM fitting as the initial parameters, the Hamiltonian parameters were fitted iteratively. The calculated and experimental energy levels for Yb^{3+}:$RETaO_4$ are consistent, and the maximal mean-root-square deviation is only 2.84 cm^{-1}, indicating that the method is effective to determine the Hamiltonian parameters of Yb^{3+} in low-symmetry crystalline sites.

Keywords: crystal field parameter, rare earth, X-ray diffraction, Yb^{3+}:$RETaO_4$

PACS: 71.70.Ch, 61.66.Fn, 61.10.–I, 78.60.–b **DOI:** 10.1088/1674-1056/22/6/067105

1. Introduction

Yb^{3+}-activated materials are an important laser medium in high-average power, ultrashort and tunable solid state lasers pumped by laser diodes (LDs), due to their simple energy level structure and relative freedom from quantum defects, which together result in favorable characteristics such as low thermal load, no deleterious up-conversion, cross relaxation, and excited state absorption, as is typical for the other rare-earth ions such as Nd^{3+}, Er^{3+}, Ho^{3+}. On the other hand, the broad absorption band is advantageous to decreasing the dependence on the work temperature control for LD, allowing the laser efficiency to be improved. Their broad emission band is desirable for the ultrashort lasers and tunable lasers, which have many important applications in the fields of machining, biology, medicine, and so on.

It is commonly hoped that Yb^{3+} at low-symmetry sites can be used to enhance a material′s crystal field splitting in order to decrease the effects of the thermal population of the laser terminal state of Yb^{3+}. If Kramers′ degeneracy is not considered, the maximum number of the crystal field energy levels is fourteen, which is far fewer than the usual number of crystal field parameters. Hence it is not so easy to determine the crystal field parameters and spin-orbital coupling parameter ξ, which is essential for the further study of the wavefunctions, transition probabilities, and nonradiative transitions of lattice vibrations. For example, the site symmetry of Yb^{3+} in Gd_2SiO_5 is C_1, and the number of the independent crystal field parameter is twenty-seven. If ξ is considered, the number of Hamiltonian parameters is twenty-eight, which is twice the number of crystal field splitting levels.

It has been found that Yb^{3+}-doped M-phase $RETaO_4$ (Yb^{3+}:$RETaO_4$, RE = Gd, Y, and Sc) has wide and strong absorption and emission bands, and these materials have attracted some interest due to their promising applications in both ultrashort and tunable lasers. For example, Yb^{3+}:$GdTaO_4$ has stronger and broader absorption and emission than Yb^{3+}:YAG, and its monocrystalline form can be grown by the Czochralski method, all of which indicates that it is very promising for application in novel all-solid state ultrashort lasers and tunable lasers.

Based on the above considerations, this work provides a method to determine the Hamiltonian parameters of Yb^{3+} in low-symmetry sites. We also prepared Yb^{3+}:$RETaO_4$ samples, determined their crystal structure, measured their photoluminescence spectra at 8k, and determined their crystal field parameters. The calculated crystal energy levels are very consistent with the experimental energy levels, which indicates that the fitting method is valuable for determining the Hamiltonian parameters of Yb^{3+} in low-symmetry sites.

2. Method to determine Hamiltonian parameters for Yb^{3+} with low symmetry in crystals

The difference f_i between the experimental and calculated energy levels, which are labeled as E_i^{exp} and E_i^{cal}

*Project supported by the National Natural Science Foundation of China (Grant Nos. 90922003, 51172236, and 50872135) and the Knowledge Innovation Program of the Chinese Academy of Sciences (Grant No. YYYJ-1002).

†Corresponding author. E-mail: zql@aiofm.ac.cn

© 2013 Chinese Physical Society and IOP Publishing Ltd

$(x_1,\ldots,x_n)$ $(i=1,\ldots,m)$ can be expressed as

$$f_i = E_i^{\exp} - E_i^{\mathrm{cal}}(x_1,\ldots,x_n), \tag{1}$$

where $x^{\mathrm{T}} = (x_1,\ldots,x_n)$, $x_1,\ldots,x_n$ stand for the free rare-earth ion Hamiltonian parameters, the real and imaginary parts of the crystal field parameters B_q^k. The Hamiltonian of the free ion Yb^{3+} has only the spin–orbit interaction parameter ξ. This can be used to minimize the following equation for fitting the crystal field energy levels by adjusting the variable $\boldsymbol{x}$,

$$\phi = \frac{1}{2}\boldsymbol{f}(x)^{\mathrm{T}}\boldsymbol{f}(x) = \frac{1}{2}\sum_{i=1}^{m}(E_i^{\exp} - E_i^{\mathrm{cal}}(\boldsymbol{x}))^2, \tag{2}$$

where $\boldsymbol{f}^{\mathrm{T}}(\boldsymbol{x}) = (f_1(\boldsymbol{x}),\ldots,f_m(\boldsymbol{x}))$, and the superscript T stands for the transpose operation on a matrix or vector. According to the derivation of the over-determined Levenberg–Marquardt iteration with $m > n$,[1] the under-determined Levenberg–Marquardt iteration formula with $m < n$, which has the same expression as the over-determined case, can be obtained as the following:

$$\boldsymbol{x}^{k+1} = \boldsymbol{x}^k - \hat{G}(\boldsymbol{x}^k)\nabla\phi(\boldsymbol{x}^k), \quad k = 0,1,\ldots, \tag{3}$$

where k is the iteration,

$$\hat{G}(\boldsymbol{x}^k) = D\boldsymbol{f}(\boldsymbol{x}^k)^{\mathrm{T}}D\boldsymbol{f}(\boldsymbol{x}^k) + \mu_k\boldsymbol{I}, \tag{4}$$

$$\nabla\phi(\boldsymbol{x}^k) = D\boldsymbol{f}(\boldsymbol{x}^k)^{\mathrm{T}}\boldsymbol{f}(\boldsymbol{x}^k), \tag{5}$$

where μ_k is a damping factor of the k-th iteration, $\boldsymbol{I}$ is a unit matrix of $n \times n$, and

$$D\boldsymbol{f}(\boldsymbol{x}^k) = \begin{pmatrix} \frac{\partial f_1}{\partial x_1} & \frac{\partial f_1}{\partial x_2} \cdots & \frac{\partial f_1}{\partial x_n} \\ \vdots & \ddots & \vdots \\ \frac{\partial f_m}{\partial x_1} & \frac{\partial f_m}{\partial x_2} \cdots & \frac{\partial f_m}{\partial x_n} \end{pmatrix}. \tag{6}$$

The key part of this iterative method is to compute the derivative of the eigenvalues of the Hamiltonian matrix with respect to its parameters, whose numerical calculation method has been given by Zhang.[2] In order to obtain the correct numeric derivative of the Hamiltonian matrix, some details are given here. The Hamiltonian matrix $\boldsymbol{H}$ with a parameter P_i, with the corresponding angular part matrix $\boldsymbol{M}^i$, and the other parameters O_t with the corresponding angular part matrix $\boldsymbol{M}^t$, can be expressed as

$$\boldsymbol{H} = P_i\boldsymbol{M}^i + \sum_t O_t\boldsymbol{M}^t. \tag{7}$$

The derivatives α-th of the eigenvalue E^α of $\boldsymbol{H}$ with the parameter P_i can be calculated by

$$\frac{\partial}{\partial P}E^\alpha \approx \frac{D\left\{\left[(P_i+\varepsilon)\boldsymbol{M}^i + \sum_t O_t\boldsymbol{M}^t\right]\right\}_\alpha - D\left\{\left[(P_i-\varepsilon)\boldsymbol{M}^i + \sum_t O_t\boldsymbol{M}^t\right]\right\}_\alpha}{2\varepsilon}, \tag{8}$$

where $D\{\boldsymbol{A}\}$ stands for the operation to diagonalize the matrix $\boldsymbol{A}$ and arrange its eigenvalues in descending or ascending order, the subscript α stands for the α-th value of the sorted eigenvalues, and ε is a small quantity such as 0.001 in the same units as the Hamiltonian parameters. We do this because the matrix eigenvalues are evaluated by an iteration process, and the order of the eigenvalues cannot be fixed by the form of the same parameterized Hamiltonian matrix.

It is important to take a set of sufficiently good Hamiltonian parameters as reasonable initial values. It is fortunate for us that the superposition model[3,4] can give a good start. The superposition model uses only two or three parameters to fit crystal field splitting, depending on the site symmetry of the magnetic ion, and generally an acceptable fitting to the low-symmetry crystal field energy levels can be obtained.

In summary, the fitting procedure to the crystal field splitting with low symmetry can be done as follows.

Step 1 Use the superposition model to fit crystal field splittings and obtain the initial crystal field parameters.

Step 2 Use Lvenberg–Marquardt iteration to refine the crystal field parameters, whose numerical derivatives of eigenvalues are calculated by Eq. (8).

3. Preparation and structural determination for Yb^{3+}: $RETaO_4$

The 5-at%Yb^{3+}:$GdTaO_4$ and 5-at%Yb^{3+}:$ScTaO_4$ were prepared by a high temperature solid state reaction method. Yb_2O_3, Gd_2O_3, Y_2O_3, Sc_2O_3, Ta_2O_5 with purity 99.999% were used as the raw materials, and weighed according to the constituent ratio of $Yb_{0.05}Gd_{0.95}TaO_4$ and $Yb_{0.05}Sc_{0.95}TaO_4$, then mixed and ground thoroughly with an agate mortar and pestle. The mixtures were calcined at 1500 degrees Celsius for 72 hours. After the samples were cooled down to room temperature, they were thoroughly re-ground as polycrystalline powder and used as an X-ray diffraction (XRD) measurement samples. The 1-at%Yb^{3+}:$YTaO_4$ polycrystalline powder was prepared by grinding the single crystal of 1-at%Yb:$YTaO_4$ grown by the Czochralski method.[5] Their X-ray diffraction data were obtained by a Philips X′pert PRO X-ray diffractometer with CuK_α radiation ($\lambda = 0.15405$ nm) at room temperature.

The collected XRD data were used to perform Rietveld refinement by GSAS,[6] during which the structural parameters of M–$GdTaO_4$, M–$YTaO_4$, and M′–$ScTaO_4$[7] were taken

as the corresponding initial structural parameters.

M–$GdTaO_4$ and M–$YTaO_4$ belong to space group $I12/a1$ (No. 15).[8] Gd and Ta occupy the Wyckoff site $4e(1/4, y, 0)$ with symmetry C_2 and the principal axis [010]. Two kinds of O occupy two general Wyckoff sites $8f(x, y, z)$, respectively.

M′–$ScTaO_4$ has space group $P12/a1$ (No. 13),[9] Ta occupies the Wyckoff site $2e(1/4, y, 0)$ with symmetry C_2 and the principal axis [010]. Sc occupies the Wyckoff site $2f(1/4, y, 1/2)$ with symmetry C_2 and the principal axis [010]. Two kinds of O occupy two general sites $4g(x, y, z)$, respectively.

The dopant Yb^{3+} should replace Gd^{3+} in the lattice due to its similar radius and charge of Yb^{3+} with Gd^{3+}, so Yb^{3+} was arranged to occupy site $4e(1/4, y, 0)$ in M–$GdTaO_4$, M–$YTaO_4$ and $2f(1/4, y, 1/2)$ in M′–$ScTaO_4$. The calculated and experimental XRD curves are shown in Figs. 1–3, the fit residuals R_p, weighted residuals R_{wp}, and D_{wd}, which is a statistical measure of the serial correlation in the powder pattern differences, are listed in Table 2. The differences between the fitted and calculated curves, R_p and R_{wp} indicate that the calculated XRD curves are very consistent with the experimental curves. The values of D_{wd} are also reasonable. All of this shows that the obtained structural parameters are reasonable. The lattice parameters and densities are listed in Table 1, atomic fractional coordinates are listed in Table 2, in which the temperature factor of each atom is also listed.

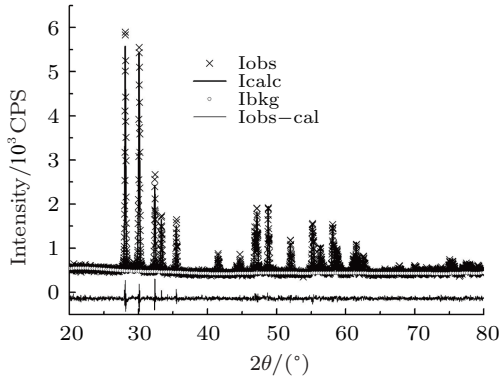


Fig. 1. Experimental and calculated curves, their difference and background curve for XRD of (5 at%)Yb:$GdTaO_4$, which are labeled Iobs, Ical, Iobs-cal, and Ibkg, respectively.

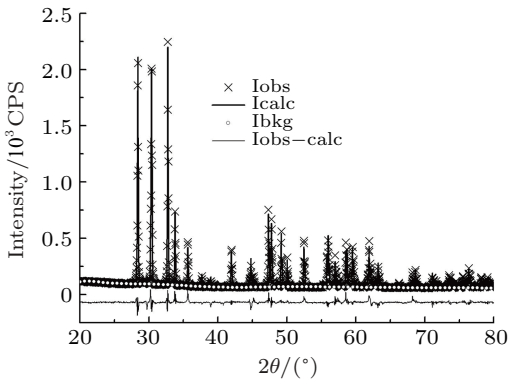


Fig. 2. Experimental and calculated curves, their difference and background curve for XRD of (1 at%)Yb:$YTaO_4$, which are labeled Iobs, Ical, Iobs-cal, and Ibkg, respectively.

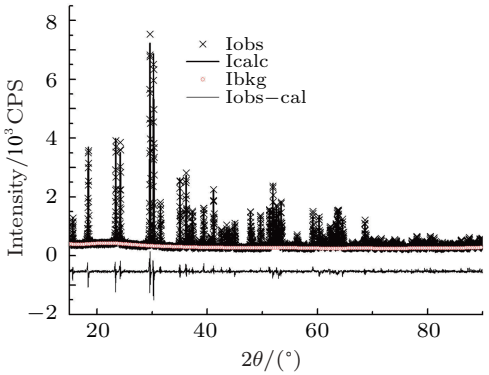


Fig. 3. (color online) The experimental, calculated, their difference and background curves for XRD of (5 at%)Yb:$ScTaO_4$, which were labeled by Iobs, Ical, Iobs-cal, and Ibkg, respectively.

Table 1. Lattice parameters and calculated densities of M–$GdTaO_4$, M–$YTaO_4$, and M′–$ScTaO_4$ from Rietveld refinements.

	M–$GdTaO_4$	M–$YTaO_4$	M′–$ScTaO_4$
$a/10^{-1}$ nm	5.399036	5.321914	5.119984
$b/10^{-1}$ nm	11.053077	10.921438	5.673244
$c/10^{-1}$ nm	5.080405	5.051231	4.815242
β/(°)	95.614	95.5302	91.708
Density/g· cm^{-3}	8.871	7.607	7.039

Yb^{3+} atoms in M–$GdTaO_4$, M–$YTaO_4$, which occupy the sites of Gd or Y, have eight coordinate atoms with four kinds of spacing, while in M′–$ScTaO_4$, Yb^{3+} occupies the site of Sc and has six coordinate atoms with three kinds of spacing. The orthogonal coordinates for Yb^{3+} and its ligands, which are needed to fit the crystal field splitting levels with the superposition model, are listed in Table 3. The polyhedron whose center is Yb^{3+} and O^{2-} ligands in M–$GdTaO_4$ and M–$YTaO_4$ are eight oxygen ions in a dodecahedron (Fig. 4, which can be seen as the result of distorting a cubic, in which eight oxygen ions lie at the corners of a cubic, and the torsion angles are listed in Table 4. The average distances $\overline{d}$ between the central ion Yb^{3+} and the ligands and the root-mean-square deviation $\delta = \sqrt{\sum_{i=1}^{8}(d_i - \overline{d_i})^2/8}$ are also listed in Table 5. It can be seen from these quantities that the distortion degree of dodecahedron YbO_8 in M–Yb^{3+}:$GdTaO_4$ is much stronger than that in M–Yb^{3+}:$YTaO_4$. The central ion Yb^{3+} and six oxygen ligands form an octahedron YbO_6 (Fig. 5), which can be seen as the distorted form of a regular octahedron whose six ligands lie at the face centers of a cubic. The distortion of YbO_6 in M′–Yb^{3+}:$ScTaO_4$ is much less than those of the YbO_8 dodecahedrons in $YTaO_4$, and $GdTaO_4$. For comparison, the corresponding values of $\overline{d}$ and δ in M–$GdTaO_4$, M–$YTaO_4$, and M′–$ScTaO_4$ are also listed in Table 5, from which it can be seen that $\overline{d}$ of O–Yb/Gd in M–Yb^{3+}:$GdTaO_4$ and $\overline{d}$ of O–Yb/Y in M–Yb^{3+}:$YTaO_4$ are both less than those of O–Gd in M–$GdTaO_4$ and O–Y in M–$YTaO_4$, which is consistent with the fact that the ion radius of Yb^{3+} is less than those of Gd^{3+}

Table 2. Atomic fractional coordinates (x, y, z), temperature factors U_{iso}, residuals, and D_{wd} from Rietveld refinements to the XRD of M–(5 at%)Yb^{3+}:$GdTaO_4$, M–(1 at%)Yb^{3+}:$YTaO_4$, and M′–Yb^{3+}:$ScTaO_4$.

		x, y, z	$100U_{ij}$[a]	R_{wp}(%), R_p(%), D_{wd}
M–Yb^{3+}::$GdTaO_4$	Gd	1/4, 0.618064, 0	–1.463, 0.575, –0.910, 0.000, –0.039, 0.000	5.03, 3.99, 1.665
	Yb		–3.770, 56.165, 80.000, 0.000, –40.000, 0.000	
	Ta	1/4, 0.149522, 0	0.091, 0.950, –1.056, 0.000, –0.410, 0.000	
	O1	0.109236, 0.459261, 0.198679	0.173, 2.685, 23.869, –6.689, –17.782, 5.661	
	O2	–0.031921, 0.71572, 0.266239	–2.219, 2.948, –3.995, 2.325, 3.962, –0.725	–
M–Yb^{3+}:$YTaO_4$	Y	1/4, 0.591157,0	1.672	8.36, 6.09, 0.703
	Yb	1/4, 0.591157,0	1.672	
	Ta	1/4, 0.118171, 0	2.422	
	O1	–0.055106, 0.302336, 0.255515	8.282	
	O2	0.052498, 0.532905, 0.258220	3.916	
M′–Yb^{3+}:$ScTaO_4$	Sc/Yb	1/4, 0.320932, 1/2	5.202	8.44, 6.45, 0.913
	Ta	1/4, 0.821389, 0	4.483	
	O1	0.420893, 0.107321, 0.217227	8.438	
	O2	0.913061, 0.380402, 0.269953	6.038	

[a] U_{ij} for M–Yb:$GdTaO_4$ stands for U_{11}, U_{22}, U_{33}, U_{12}, U_{13}, U_{23}, and for M–$YTaO_4$ and M′–$ScTaO_4$ stand for U_{iso}, respectively.

Table 3. The orthogonal coordinates (x, y, z) in 10^{-1} nm for Yb^{3+} and its ligands in M–$GdTaO_4$, M–$YTaO_4$, and M′–$ScTaO_4$.

Atom	(X, Y, Z) in M–$GdTaO_4$	(X, Y, Z) in M–$YTaO_4$	(X, Y, Z) in M′–$ScTaO_4$
Yb^{3+}	1.3498, 6.8315, 0	1.3305, 6.4563, 0	1.2082, 1.8207, 2.4066
O1	0.491, 5.0762, 1.0045	0.1537, 5.8201, 1.2983	0.2927, 0.6089, 3.7676
O2	3.1905, 5.9768, 1.0045	2.8146, 5.1013, 1.2983	2.1238, 0.6089, 1.0455
O3	2.7557, 8.6261, 1.1819	2.2433, 7.6195, 1.2847	2.0761, 3.5151, 1.2993
O4	–0.3047, 7.9535, 1.3461	0.1743, 8.7627, 1.2292	0.3404, 3.5151, 3.5138
O1′	–0.491, 5.9768, –1.0045	–0.1537, 5.1013, –1.2983	–0.4839, 2.1581, 1.2993
O2′	2.2085, 5.0762, –1.0045	2.5073, 5.8201, –1.2983	2.9003, 2.1581, 3.5138
O3′	3.0042, 7.9535, –1.3461	2.4867, 8.7627, –1.2292	
O4′	–0.0562, 8.6261, –1.1819	0.4177, 7.6195, –1.2847	

Table 4. The plane torsion angles of the YbO_8 polyhedron in M–Yb^{3+}:$GdTaO_4$ and Yb^{3+}:$YTaO_4$, YbO_6 in M′–Yb^{3+}:$ScTaO_4$.

Torsion angle/(°)	M–Yb^{3+}:$GdTaO_4$	M–Yb^{3+}:$YTaO_4$	Torsion angle/(°)	M′–Yb^{3+}:$ScTaO_4$
O1–O2–O3–O4	2.593	1.503	O1–O2–O3–O4	–4.172
O1′–O2′–O3′–O4	2.297	1.416		
O1–O1′–O2′–O2	–32.826	–19.822		
O2–O2′–O3′–O3	–27.622	–18.978		

Table 5. The distance d in 10^{-1} nm between the central ion Yb^{3+} and oxygen ligands in Yb^{3+}-doped and undoped M–$GdTaO_4$ and $YTaO_4$, YbO_6 in M′–$ScTaO_4$.

Atom	d (10^{-1} nm) in Yb^{3+} -doped/undoped M–$GdTaO_4$	d (10^{-1} nm) in Yb^{3+} -doped/undoped -Yb^{3+}:$YTaO_4$	d (10^{-1} nm) in Yb^{3+} -doped/undoped M′–$ScTaO_4$
O1	2.1972/2.4006	1.8642/2.3680	2.0394/2.1128
O2	2.2644/2.3368	2.3925/2.2753	2.0394/2.1128
O3	2.5679/2.4423	1.9587/2.3852	2.2024/2.1752
O4	2.4100/2.3830	2.8578/2.3133	2.2024/2.1752
O1′	2.2645/2.4006	2.3926/2.2753	2.0501/2.1099
O2′	2.1971/2.3368	1.8642/2.3680	2.0501/2.1099
O3′	2.4100/2.3830	2.8578/2.3133	
O4′	2.5679/2.4423	1.9587/2.3852	
$\bar{d}/10^{-1}$ nm	2.3599/2.3907	2.2683/2.3355	2.0973/2.13263
$\delta/10^{-1}$ nm	0.05043/0.01338	0.13943/0.01545	0.03782/ 0.01230

and Y^{3+}, and when the smaller-radius ions occupy the sites of the greater-radius ions the crystal cell volume decreases. Although $\overline{d}$ of Yb/Sc–O in M′–Yb:$ScTaO_4$ is larger than that of Sc–O in M′–$ScTaO_4$, the distances of O3–Yb/Sc and O4–Yb/Sc are larger than those of O3–Sc and O4–Sc, which results in the doped material′s larger cell volume. All of the δ values for M–Yb^{3+}:$GdTaO_4$, M–Yb^{3+}:$YTaO_4$, and M′–Yb^{3+}:$ScTaO_4$ are larger than those of the corresponding undoped compounds, which means Yb-doping causes further distortion of their polyhedra of rare-earth ions.

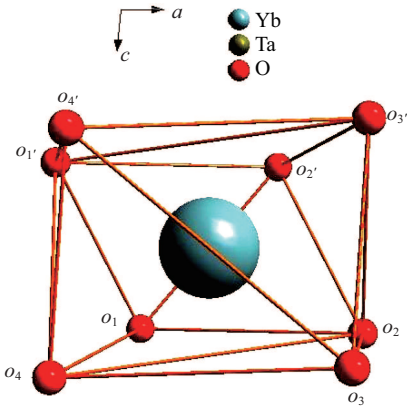


Fig. 4. (color online) Polyhedron formed by central ion Yb^{3+} and its ligands O^{2-} in M–Yb:$GdTaO_4$ and M–Yb:$YTaO_4$, which is viewed from direction [010].

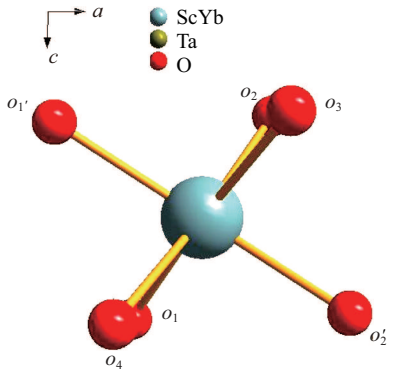


Fig. 5. (color online) Octahedron formed by central ion Yb^{3+} and its ligands O^{2-}, which is viewed from direction [010].

4. Hamiltonian parameter determination of Yb^{3+}:$RETaO_4$

4.1. Energy level fitting by superposition model

The superposition model (SM) is based on the following postulates:[1] (i) the crystal field acting on the open-shell electrons of a paramagnetic ion is the resultant of a sum of contributions coming from individual ions in the crystal. (ii) Only contributions from the neighboring ions, namely ligands, are taken into account. (iii) Each single-ion contribution in the sum is axially symmetric about the line joining its center to that of the paramagnetic ion. (iv) Single-ligand contributions are dependent only on the nature of the ligand and its distance from the paramagnetic ion, and do not depend on other properties of the host crystal. Then, the crystal field parameter B_q^k can be expressed by

$$B_q^k = \sum_L \overline{B_k}(R_L) g_{k,q}(\theta_L, \varphi_L), \tag{9}$$

where L stands for the L-th ligand, and R_L, $\bar{B}_k(R_L)$ and $g_{k,q}$ stand for the distance of L-th ligand, its intrinsic crystal field parameter, and coordinate factor. The crystal field equation (9) is a little different from that in Refs. [3] and [4], where B_q^k is complex generally and $g_{k,q}$ is calculated from

$$g_{k,q}(\theta_L, \varphi_L) = \sqrt{\frac{4\pi}{2k+1}} \mathrm{Y}_q^k(\theta_L, \varphi_L), \tag{10}$$

where $\mathrm{Y}_q^k(\theta_L, \varphi_L)$ is the spherical harmonic function. If there are several ligand distances with the shortest R_0, it is generally assumed that $\bar{B}_k(R_L)$varies with R_L as[3]

$$\overline{B_k}(R_L) = \overline{B_k}(R_0) \left(\frac{R_0}{R_L}\right)^{t_k}. \tag{11}$$

And t_k can be determined experimentally or t_2, t_4, t_6 taken to be 3, 5, and 7, respectively. Let $\overline{B_k}(R_0) \equiv \overline{B_k}$ for convenience. Taking Eq. (11) into Eq. (9), the following is obtained

$$B_q^k = \overline{B_k} \sum_L \left(\frac{R_0}{R_L}\right)^{t_k} g_{k,q}(\theta_L, \varphi_L). \tag{12}$$

The Hamiltonian $\hat{H}$ for Yb^{3+} in $RETaO_4$ can be expressed as

$$\hat{H} = \xi \boldsymbol{S} \cdot \boldsymbol{L} + \sum_{k,q} B_q^k C_q^k, \tag{13}$$

where ξ is the spin-orbital parameter, $\boldsymbol{S}$ and $\boldsymbol{L}$ are spin and orbital angular moment operators, and C_q^k expresses the angular dependence of the crystal field.

The site symmetry of Yb^{3+} in $RETaO_4$ is C_2, it has three intrinsic parameters $\overline{B_2}(R_0)$, $\overline{B_4}(R_0)$, and $\overline{B_6}(R_0)$, and fifteen non-vanishing crystal field parameters B_q^k with $(k,q) =$ (2,±2), (2,0), (4,±4), (4,±2), (4, 0), (6, ±6), (6, ±4), (6, ±2), (6, 0). The independent crystal parameters are B_q^k with (k, q) = (2,2), (2,0), (4, 4), (4, 2), (4, 0), (6, 6), (6, 4), (6, 2), (6, 0), of which B_0^k (k = 2, 4, 6) are real and the others are complex. So the independent crystal parameters have fifteen real parameters to be determined.

During our calculation, the principal axis of the crystal field parameters is along the [001] direction. The principal axis of the original ligand coordinates $\boldsymbol{X}^{\mathrm{T}} = (x, y, z)$ in Table 3 is along the [010] direction, on which a transformation

$$\boldsymbol{\tau} = \begin{pmatrix} 0 & 0 & 1 \\ 1 & 0 & 0 \\ 0 & 1 & 0 \end{pmatrix}$$

should be applied to make their principal axis along the [001] direction and transformed $\boldsymbol{X}'$ is

$$\boldsymbol{X}' = \tau X. \tag{14}$$

The Levenberg–Marquardt iteration is used to fit the intrinsic parameters $\overline{B_k}(R_0)$ to the crystal field levels, which is similar to the method described in Section 2 and Ref. [2]. The Hamiltonian matrix is calculated with the base set $\{|\mathrm{SLJM}\rangle\} = \{|^2F_{7/2},7/2\rangle,\ |^2F_{7/2},5/2\rangle,\ldots,\ |^2F_{7/2},-7/2\rangle, |^2F_{5/2},5/2\rangle,\ |^2F_{5/2},3/2\rangle,\ldots,\ |^2F_{5/2},-5/2\rangle\}$. The residual R and root-mean-square deviation σ are used to characterize the consistency between the experimental and calculated levels by

$$R = \sqrt{\frac{\sum_{i=1}^{m}(E_i^{\mathrm{exp}} - E_i^{\mathrm{cal}}(x))^2}{\sum_{i=1}^{m}(E_i^{\mathrm{exp}})^2}}, \tag{15}$$

$$\sigma = \sqrt{\frac{\sum_{i=1}^{m}(E_i^{\mathrm{exp}} - E_i^{\mathrm{cal}}(x))^2}{m-3}}. \tag{16}$$

The number 3 in Eq. (16) stands for the number of $\overline{B_k}(R_0)$.

The initial variable values of SM $\boldsymbol{x}^{\mathrm{T}} = (\xi, \overline{B_2}, \overline{B_4}, \overline{B_6})$ for M–Yb^{3+}:$GdTaO_4$, M–Yb^{3+}:$YTaO_4$, and M′–Yb^{3+}:$ScTaO_4$ are (2900, 10, 100, 200), (2900, 100, 100, 100), and (2900, 100, 100, 100), maximal iteration loop number and search number for the damping factor of Levenberg–Marquardt iteration are both 20. After iterations 5, 12, and 7, the obtained $\boldsymbol{x}^{\mathrm{T}}$ are (2907, 344, 818, 275), (2908, 969, 664, 814), and (2899, 2649, 612, 383), respectively. ξ, $\overline{B_k}$, and B_q^k for M–Yb^{3+}:$GdTaO_4$, M–Yb^{3+}:$YTaO_4$, and M′–Yb^{3+}:$ScTaO_4$ are listed in Table 6. The experimental and calculated crystal field levels, R and σ of Yb^{3+}:$RE$$TaO_4$ are listed in Table 7. It can be seen that the residuals R and σ for M–Yb^{3+}:$GdTaO_4$, M–Yb^{3+}:$YTaO_4$ are very close—their R values are both 0.29%, and their σ values are 23.89 cm^{-1} and 23.68 cm^{-1}, respectively. If $\boldsymbol{x}^{\mathrm{T}} = (\xi, \overline{B_2}, \overline{B_4}, \overline{B_6}) = (2900, 100, 100, 100)$ are taken as the initial iteration parameters of M–Yb^{3+}:$GdTaO_4$, similar results with the same R and σ values are obtained, and the final $\boldsymbol{x}^{\mathrm{T}} = (2907, 358, 816, 283)$. If $\boldsymbol{x}^{\mathrm{T}} = (\xi, \overline{B_2}, \overline{B_4}, \overline{B_6}) = (2900, 10, 100, 200)$ are taken as the initial iteration parameters of M–Yb^{3+}:$YTaO_4$, R and σ would be decreased greatly, that is 0.16% and 12.86 cm^{-1}, and the final $\boldsymbol{x}^{\mathrm{T}} = (2909, -792, 753, 602)$. It seems that the negative $\overline{B_2}$, which is –792 cm^{-1}, is unreasonable. Many initial values of $\boldsymbol{x}^{\mathrm{T}}$ were tried for M–Yb^{3+}:$YTaO_4$, and results similar to (2908, 969, 664, 814) were always obtained. So it is believed that $\boldsymbol{x}^{\mathrm{T}} = (2908, 969, 664, 814)$ is reasonable for M–Yb^{3+}:$YTaO_4$. It seems satisfactory for the results of fitting M′–Yb^{3+}:$ScTaO_4$ with R and σ 0.16% and 13.44 cm^{-1}, respectively. But the intrinsic crystal parameter $\overline{B_2}$ of M′–Yb^{3+}:$ScTaO_4$ is much larger than that of M–Yb^{3+}:$GdTaO_4$ and M–Yb^{3+}:$YTaO_4$, which may result from the ligand difference and crystal structure, that is, the space group of M–Yb^{3+}:$GdTaO_4$ and M–Yb^{3+}:$YTaO_4$ is $I12/a1$, but that of M′–$ScTaO_4$ is $P12/a1$, the ligand number of M–Yb^{3+}:$GdTaO_4$ and M–Yb^{3+}:$YTaO_4$ is eight, but that of M′–Yb^{3+}:$ScTaO_4$ is 6. On the other hand, the Yb–O polyhedron distortion degree of M–Yb^{3+}:$GdTaO_4$ and M–Yb^{3+}:$YTaO_4$ is stronger than that of M′–Yb^{3+}:$ScTaO_4$.

Table 6. $\overline{B_k}$ and B_q^k of Yb^{3+}:$RE$$TaO_4$ obtained by SM fitting in unit cm^{-1}.

	M–Yb^{3+}:$GdTaO_4$	M–Yb^{3+}:YTaO4	M′–Yb^{3+}:$ScTaO_4$
ξ	2907.050	2908.274	2898.837
$\overline{B_2}$	344.237	968.596	2649.108
$\overline{B_4}$	817.863	663.723	611.583
$\overline{B_6}$	275.071	814.249	383.026
B_2^2	–229.082+15.154I	276.814–154.767I	–201.696–117.657I
B_0^2	143.882	–342.600	–606.910
B_4^4	–730.448–429.766I	–808.022+10.055I	–656.456–653.216I
B_2^4	30.228–602.424I	107.534+502.598I	423.009–1176.547I
B_0^4	–1034.515	–598.421	–423.750
B_6^6	170.127+73.731I	–263.921+393.789I	205.131–55.980I
B_4^6	–320.145–96.934I	–638.288+245.245I	–242.726–166.938I
B_2^6	107.895–180.006I	–113.833–97.159I	–97.035+187.296I
B_0^6	–23.644	589.192	–116.0389

According to Table 6, it can be seen that the signs of real and imaginary parts for B_q^k of M–Yb^{3+}:$GdTaO_4$, M–Yb^{3+}:$YTaO_4$, and M′–Yb^{3+}:$ScTaO_4$ are not consistent with each other. Because their intrinsic crystal parameter signs the $\overline{B_k}$ values are the same, the crystal field parameter signs were decided by their coordination factor $g_{k,q}(\theta_L, \varphi_L)$, which may mean that the crystal field parameter signs are very sensitive to

Table 7. The experimental and calculated crystal field energy levels, R and σ of Yb^{3+}:$RE$$TaO_4$ by fitting with SM.

M–Yb^{3+}:$GdTaO_4$		M–Yb^{3+}:$YTaO_4$		M′–Yb^{3+}:$ScTaO_4$	
$E^{\mathrm{cal}}/\mathrm{cm}^{-1}$	$E^{\mathrm{exp}}/\mathrm{cm}^{-1}$	$E^{\mathrm{cal}}/\mathrm{cm}^{-1}$	$E^{\mathrm{exp}}/\mathrm{cm}^{-1}$	$E^{\mathrm{cal}}/\mathrm{cm}^{-1}$	$E^{\mathrm{exp}}/\mathrm{cm}^{-1}$
0	0	0	0	0	0
260	283	262.92	284	263.36	246
421.48	417	410.41	416	460.74	468
611.16	607	632.07	609	820	811
10266.77	10285	10287.85	10288	10264.14	10269
10494.92	10460	10499.69	10471	10450.01	10429
10751.88	10779	10756.8	10788	10912.19	10914
$R = 0.29\%$ $\sigma = 23.89\ \mathrm{cm}^{-1}$		$R = 0.29\%$ $\sigma = 23.68\ \mathrm{cm}^{-1}$		$R = 0.16\%$ $\sigma = 13.44\ \mathrm{cm}^{-1}$	

the relative positions of the ligands, which depends not only on their site symmetry, but also on the relative positions of their ligands.

No obvious trend or rule for the intrinsic crystal field parameters $\overline{B_k}$ or crystal field parameters B_q^k was found from M–Yb^{3+}:$GdTaO_4$, M–Yb^{3+}:$YTaO_4$ to M′–Yb^{3+}:$ScTaO_4$, which suggests that the crystal field parameters are sensitive to the structure of their Yb–O polyhedron.

4.2. Crystal field parameter fitting

Using the crystal field parameters obtained by SM fitting as the initial parameters, the crystal field parameters of M–Yb^{3+}:$GdTaO_4$, M–Yb^{3+}:$YTaO_4$, and M′–Yb^{3+}:$ScTaO_4$ were fitted to their experimental energy levels by Levenberg–Marquardt, as described previously. The initial orbital-spin coupling parameter ξ for all crystals is 2900 cm^{-1}, the maximal iteration and search-damping factor numbers are 20 and 20, respectively. The obtained ξ and B_q^k, calculated and experimental energy levels are listed in Table 8 and Table 9, respectively. The values of R and σ decreased greatly, the consistency between the calculated and experimental energy levels is very good. But some of the real and imaginary part signs of the crystal field parameters for M–Yb^{3+}:$GdTaO_4$ and M–Yb^{3+}:$YTaO_4$ are not the same as those given by SM fitting, such as B_6^6 and B_2^6 for M–Yb^{3+}:$GdTaO_4$, B_2^4 and B_2^6 for M–Yb^{3+}:$YTaO_4$. As mentioned before, direct fitting to the energy levels for M′–Yb^{3+}:$ScTaO_4$ gives the closed crystal field parameters and orbital-spin coupling parameter ξ, which indicates that SM fitting gives good initial Hamiltonian parameters. There is still no obvious trend which can be seen from the crystal field parameters obtained by direct fitting from M–Yb^{3+}:$GdTaO_4$, M–Yb^{3+}:$YTaO_4$, and M′–Yb^{3+}:$ScTaO_4$.

The second-order moment σ_2^2, crystal field strength parameter N_v, and s_k^2 were also computed through the crystal field parameters obtained by direct fitting. It can be seen that the values of N_v for M–Yb^{3+}:$GdTaO_4$ and M–Yb^{3+}:$YTaO_4$ are 2038 cm^{-2} and 2019 cm^{-2}, and are very close, and the value 2742 cm^{-2} of M′–Yb^{3+}:$ScTaO_4$ is smaller, indicating that the crystal-field strength of M–Yb^{3+}:$GdTaO_4$ and M–Yb^{3+}:$YTaO_4$ are nearly the same, and that of M′–Yb^{3+}:$ScTaO_4$ is the strongest.

The wavefunctions and energy levels of Yb^{3+} in M–Yb^{3+}:$GdTaO_4$, M–Yb^{3+}:$YTaO_4$, and M′–Yb^{3+}:$ScTaO_4$ can be calculated through these parameters. The crystal field splitting of Yb^{3+} in M–Yb^{3+}:$GdTaO_4$ is labeled by the irreducible symbol of point group C_2 and shown in Fig. 6, which is the leading component of the corresponding wavefunction, similar

Table 8. B_q^k of Yb^{3+}:*RE*TaO_4 obtained by direct fitting in cm^{-1}.

	M–Yb^{3+}:$GdTaO_4$	M–Yb^{3+}:$YTaO_4$	M′–Yb^{3+}:$ScTaO_4$
ξ	2907.569	2909.695	2899.072
B_2^2	–360.709+251.041i	282.444–358.100i	–157.203–168.600i
B_0^2	318.619	325.189	–731.210
B_4^4	–697.962–145.129i	–654.746+324.814i	–531.975–451.898i
B_2^4	503.534–152.620i	–475.378+155.477i	508.556–1171.039i
B_0^4	–579.240	–503.567	–424.907
B_6^6	286.561–64.242i	–130.420+223.066i	160.657–18.936i
B_4^6	–166.573–19.093i	–124.300+90.567i	–209.882–114.359i
B_2^6	121.216+10.717i	–129.970+46.964i	–85.213+260.233i
B_0^6	–137.409	–89.024	–148.177
s_2^2	97557	104354	185686
s_4^2	211736	202476	354643
s_6^2	21324	17458	57943
$\sigma_2^2(^2F_{5/2})$	42104	69930	77507
$\sigma_2^2(^2F_{7/2})$	67964	43731	124546
N_v	2038	2019	2742

Table 9. The experimental and calculated crystal field levels, R and σ of Yb^{3+}:*RE*TaO_4.

M–Yb^{3+}:$GdTaO_4$		M–Yb^{3+}:$YTaO_4$		M′–Yb^{3+}:$ScTaO_4$	
E^{cal}/cm^{-1}	E^{exp}/cm^{-1}	E^{cal}/cm^{-1}	E^{exp}/cm^{-1}	E^{cal}/cm^{-1}	E^{exp}/cm^{-1}
0	0	0	0	0	0
283.01	283	283.66	284	246	246
417.99	417	418.23	416	468	468
608.49	607	611.57	609	811	811
10286.02	10285	10289.69	10288	10269	10269
10460.65	10460	10472.11	10471	10429	10429
10779.25	10779	10788.6	10788	10914	10914
$R = 0.012\%$ $\sigma = 1.54$ cm^{-1}		$R = 0.022\%$ $\sigma = 2.84$ cm^{-1}		$R = 0\%$ $\sigma = 0$ cm^{-1}	

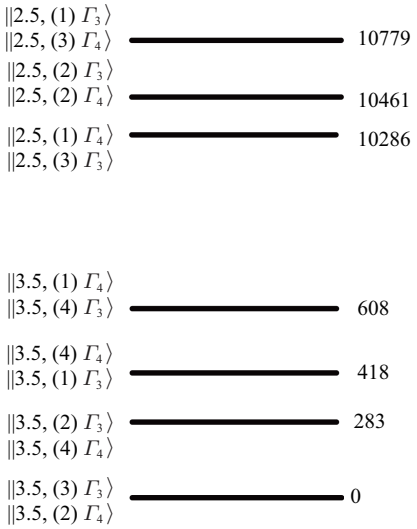


Fig. 6. Schematic diagram of the crystal field splitting of Yb^{3+} in M–Yb:$GdTaO_4$, in which the right energy level values are in cm^{-1}.

to the crystal field splitting for M–Yb^{3+}:$YTaO_4$ and M′–Yb^{3+}:$ScTaO_4$. In the energy level label $|[^{2S+1}L_J,(r)\Gamma m]\rangle$, $^{2S+1}L_J$ stands for the free-ion multiplet, r stands for the reduction multiplicity from full rotation group O_3^* to the site point group C_2, Γm is an irreducible symbol, which is identical with that of Ref. [10]. The square brackets indicate that $|^{2S+1}L_J,(r)\Gamma m\rangle$ is the leading component. Every wavefunction of each crystal field energy level is the mixture of the irreducible representation Γ_3 and Γ_4 of one dimension, and every two wavefunctions correspond to one crystal field energy level and result in double degeneration, which results from the time inversion. As a typical example, the component ratio of the wavefunction $|[3.5,(2)\Gamma_4]\rangle$ is shown as the following:

$$
\begin{aligned}
&|3.5,(1)\Gamma_3\rangle : 0.1952\%; \quad |3.5,(2)\Gamma_3\rangle : 0.0993\%;\\
&|3.5,(3)\Gamma_3\rangle : 0.2173\%; \quad |3.5,(4)\Gamma_3\rangle : 0.0518\%;\\
&|3.5,(1)\Gamma_4\rangle : 9.1319\%; \quad |3.5,(2)\Gamma_4\rangle : 38.3326\%;\\
&|3.5,(3)\Gamma_4\rangle : 17.5159\%; \quad |3.5,(4)\Gamma_4\rangle : 34.4477\%;\\
&|2.5,(1)\Gamma_4\rangle : 0.0039\%; \quad |2.5,(2)\Gamma_4\rangle : 0.0033\%;\\
&|2.5,(3)\Gamma_4\rangle : 0.001\%.
\end{aligned}
$$

It can be seen that the ratio of Γ_4 reduced from $D^{7/2}$ is up to 99.3%, which means that it can be labeled as Γ_4 unambiguously. If the reduction symbol relative to the irreducible representation D^J is omitted, every crystal field energy level can be labeled as $\Gamma_{3,4}$, which stands for the irreducible Γ_3 and Γ_4.

5. Conclusion

A method to determine the Hamiltonian parameters of Yb^{3+} in the low site symmetry of crystal, such as the orbital-spin coupling parameter and crystal-field parameters, was given. Based on the structural parameters of M–Yb^{3+}:$GdTaO_4$, M–Yb^{3+}:$YTaO_4$, and M′–Yb^{3+}:$ScTaO_4$, which were prepared by the solid-state reaction method, their structural parameters are refined by Rietveld refinement methods; their orbital-spin parameter and crystal field parameters were fitted by SM or directly. The calculated and experimental energy levels for M–Yb^{3+}:$GdTaO_4$, M–Yb^{3+}:$YTaO_4$, and M′–Yb^{3+}:$ScTaO_4$ agree very well, and the maximal mean-root-square deviation is just 2.84 cm^{-1}, which indicates that the method to determine the Hamiltonian parameters of Yb^{3+} in a low-symmetry crystal site is effective, so the obtained wavefunctions can be used to compute their spectral properties such as transition probabilities and so on.

Acknowledgement

The authors are very grateful to Profs. D. J. Newman and Betty Ng for many valuable comments and for critically reading the manuscript.

References

[1] Li Q Y, Guan Z and Bai S F 2000 *The Principles of Numeric Calculation* (Beijing: Tsinghua University Press) p. 291 (in Chinese)
[2] Zhang Q L, Ning K J, Xiao J, Ding L H, Zhou W L, Liu W P, Yin S T and Jiang H H 2010 *Chin. Phys. B* **19** 086705
[3] Newman D J and Ng B 1989 *Rep. Prog. Phys.* **52** 699
[4] Newman D J, Price D C and Runciman W A 1978 *Am. Mineral* **63** 1278
[5] Ding L H 2010 Ph. D. Dissertation (Beijing: Chinese Academy of Sciences) (in Chinese)
[6] Larson A C and Von Dreele R B 2004 *General Structure Analysis System* (Los Alamos National Laboratory Report LAUR)
[7] Keller C 1962 *Z. Anorg. Allg. Chem.* **318** 89
[8] Theo H 2005 *International Tables for Crystallography*, Volume A: *Space-Group Symmetry*, 5th edn. (Dordrecht: Sringer) p. 195
[9] Theo H 2005 *International Tables for Crystallography*, Volume A: *Space-Group Symmetry*, 5th edn. (Dordrecht: Sringer) p. 179
[10] Koster G F, Dimmock J O, Wheeler R G and Statz H 1963 *Properties of the Thirty-Two Point Groups* (Massachusetts: MIT Press) p. 103